1088 *Chem. Mater.* **2010,** *22,* 1088–1097
DOI:10.1021/cm902118m

CHEMISTRY OF MATERIALS
Article

Comparative Study of Lithium Transport Kinetics in Olivine Cathodes for Li-ion Batteries†

Nonglak Meethong,‡ Yu-Hua Kao,§ W. Craig Carter,§ and Yet-Ming Chiang*,§

‡*Khon Kaen University, Muang District, Khon Kaen, Thailand, and* §*Massachusetts Institute of Technology, Cambridge, Massachusetts, USA*

Received July 13, 2009. Revised Manuscript Received September 4, 2009

Crystallite size and composition effects on the kinetics of lithium storage in olivines are studied using potentiostatic intermittent titration tests (PITT). Here we compare undoped $Li_{1-x}FePO_4$ of 113 nm, 42 nm, and 34 nm average particle size, and three aliovalent solute doped compositions formulated for dopant substitution on the Li (M1) site with charge compensation by Li vacancies: $Li_{0.90}Mg_{0.05}FePO_4$, $Li_{0.80}Zr_{0.05}FePO_4$, and $Li_{0.70}Zr_{0.075}FePO_4$. The results first show that a diffusive component can be measured with reasonable accuracy in all samples, allowing determination of the lithium chemical diffusion coefficient D as a function of potential or state-of-charge. In addition, a method is illustrated for the separation of capacity due to diffusive transport from that due to the first-order phase transition. Using the combined analyses, the effects of particle size reduction and aliovalent doping are readily understood. Both effects contribute to a reduced lithium miscibility gap and a greater contribution to stored capacity of the (faster) diffusive process. Simultaneously, the rate of phase transformation within the miscibility gap is also increased. Highly doped samples exhibit a complete lithium solid solution at room temperature, and have 1−2 orders of magnitude higher D at potentials where significant capacity is stored. This translates to improved capacity retention at high cycling rates, albeit at the expense of reduced absolute capacity due to Li diffusion channel blocking.

Introduction

Lithium transition metal phosphate olivines have become commercially important as positive electrode materials in a new generation of lithium-ion batteries that are especially well-suited for applications requiring high power, improved safety, and long life. Recently demonstrated applications of nanoscale olivine batteries include cordless power tools, hybrid electric and all-electric vehicles, and even MW-scale grid stabilization systems.[1−3] Nanoscale olivines are furthermore an exemplar of systems in which nanoscaling causes clear and measurable differences in physical properties that can be tuned to improve practical battery performance. Known nanoscale effects include a reduction in the lithium miscibility gap with decreasing crystallite size below 100 nm.[4,5] In previous work, we have shown that the width of the miscibility gap, as measured by electrochemical titration and XRD measurements of structure vs Li composition, determines the qualitative nature of the lithium storage mechanism.[6] The rate of the first-order phase transformation that dominates the lithium storage/release process is highly correlated with the misfit strain between lithiated and delithiated phases, and therefore the width of the miscibility gap. Recent work shows that size reduction also influences the phase transformation pathway and can determine whether lithium insertion is accommodated by a crystalline−crystalline or crystalline−amorphous phase transition.[7,8] The miscibility gap has also been shown to be highly susceptible to manipulation by aliovalent doping,[9] transition cation mixing,[10,11] and Li−Fe antisite disorder.[12] However, disorder or doping that produces immobile cation species on the [010] rows of Li sites (M1 sites) can also reduce accessible capacity by blocking Li diffusion. As discussed elsewhere,[9] the impact on capacity can

†Accepted as part of the 2010 "Materials Chemistry of Energy Conversion Special Issue".

*Massachusetts Institute of Technology, 77 Massachusetts Avenue, Bldg 13, Rm. 13-4086. Phone (617) 253 6471, Fax (617) 253 6201, Email: ychiang@mit.edu.

(1) Macilwain, C. *Nature* **2006**, *444*, 17.
(2) Chu, A. Development of HEV Batteries with Lithium Iron Phosphate Cathodes. Presented at the Advanced Automotive Battery Conference, Baltimore, MD, May 15−19, 2006.
(3) www.A123Systems.com
(4) Meethong, N.; Huang, H. S.; Carter, W. C.; Chiang, Y. M. *Electrochem. Solid-State Lett.* **2007**, *10*(5), A134.
(5) Yamada, A.; Koizumi, H.; Nishimura, S.-I.; Sonoyama, N.; Kanno, R.; Yonemura, M.; Nakamura, T.; Kobayashi, Y. *Nat. Mater.* **2006**, *5*, 357.
(6) Meethong, N.; Huang, H. S.; Speakman, S. A.; Carter, W. C.; Chiang, Y. M. *Adv. Funct. Mater.* **2007**, *17*, 1115.
(7) Meethong, N.; Kao, Y.-H.; Tang, M.; Huang, H.-Y.; Carter, W. C.; Chiang, Y.-M. *Chem. Mater.* **2008**, *20*, 6189.
(8) Tang, M.; Huang, H.-Y.; Meethong, N.; Kao, Y.-H.; Carter, W. C.; Chiang, Y.-M. *Chem. Mater.* **2009**, *21*, 1557.
(9) Meethong, N.; Kao, Y. H.; Speakman, S. A.; Chiang, Y. M. *Adv. Funct. Mater.* **2009**, *19*, 1060.
(10) Yamada, A.; Kudo, Y.; Liu, K. Y. *J. Electrochem. Soc.* **2001**, *148*, A1153.
(11) Chiang, Y.-M.; Chu, A. C.; Jang, Y.-I.; Meethong, N.; Kao, Y.-H.; Riley, G. N.; Pullen, A. E.; Thomas-Alyea, K. E. Multifunctional Mixed Metal Olivines for Li-ion Batteries. WO Patent 29009758A2, Jan 15, **2009**.
(12) Gibot, P.; Casas-cabanas, M.; Laffont, L.; Levasseur, S.; Carlach, P.; Hamelet, S.; Tarascon, J.-M.; Masquelier, C. *Nat. Mater.* **2008**, *7*, 741.

 Published on Web 09/29/2009

Table 1. Six Samples for Which Lithium Storage Kinetics Are Here Compared, And Their Respective Equivalent Spherical Particle Sizes As Determined by BET Measurements of Specific Surface Area

sample	composition	particle size (nm)
1	$LiFePO_4$	113
2	$LiFePO_4$	42
3	$LiFePO_4$	34
4	$Li_{0.90}Mg_{0.05}FePO_4$	43
5	$Li_{0.80}Zr_{0.05}FePO_4$	45
6	$Li_{0.70}Zr_{0.075}FePO_4$	45

be assessed by considering the average number of blocking ions per [010] channel, under the assumption that the ends of each channel remain open for Li extraction and insertion.

Thus the lithium exchange kinetics in this class of olivines are necessarily more complex than in most intercalation compounds. In this paper, we carry out a comparative analysis of olivine materials varying systematically in particle size and composition. A good database of properties has been developed for most of the samples used here through previous work.[4,6,7,9] The results obtained here permit an improved understanding of the lithium storage mechanisms and critical materials design factors for improved performance. We use potentiostatic intermittent titration tests (PITT) as a primary method to explore the kinetics in the small overpotential, small incremental capacity limit. Effects such as overpotential-induced amorphization[7,8] are thereby minimized. By titrating with incremental voltages and capacities, we also avoid kinetic limitations due to electrode formulation, thickness, and density, which can dominate electrode kinetics at higher cycling rates as recent studies[13] illustrate.

Experimental Section

The samples studied are listed in Table 1. We characterized the particle sizes of the powders by measuring their specific surface area using the BET method (Brunauer, Emmett, and Teller) and computing the equivalent spherical particle size (Table 1). This gives a mean value of the particle size for each sample, but does not provide information on the size distribution. TEM observations[4] previously showed that the sample of 113 nm particle size, a "carbon added" $LiFePO_4$ powder that was commercially available (Aldrich Chemical), has a wide distribution in crystallite size. However, all of the other powders, prepared from the main starting materials $FeC_2O_4 \cdot 2H_2O$, Li_2CO_3, and $NH_4H_2PO_4$ using the procedures of ref 14, have a narrow crystallite size distribution as shown in previous studies.[4,14] The final firing of these powders was conducted at 700 °C for 6 h in Ar. In the doped samples, $MgC_2O_4 \cdot 2H_2O$ and $Zr(OC_2H_5)_4$ of reagent-grade purity were used as the source of the dopant cation.

The three undoped $Li_{1-x}FePO_4$ samples with mean particle sizes of 113, 42, and 34 nm were previously subjected to other characterization methods in the references.[4,6,7,9] Here, we used them to study the effect of crystallite size at a constant composition on the charge/discharge kinetics. Note that as the particle size varies in the sub-100 nm range, there is also a systematic variation in the width of the lithium miscibility gap, and therefore in the misfit strain between the lithiated (triphylite) and delithiated (heterosite) phases under two-phase coexistence where each phase is saturated with respect to the other.[4]

The three nanoscale, aliovalent-doped samples that were included in the study have nearly identical crystallite size, 42−45 nm. In these samples, the miscibility gap is further narrowed compared to undoped samples of the same particle size. The doped compositions have, when fully lithiated, the formula $Li_{1-nx}M^{n+}{}_xFePO_4$ (doping mechanism 1 in ref 9), in which the dopants are Mg^{2+} (5%) and Zr^{4+} (5% and 7.5%). By altering the overall cation ratios of the sample, we promote charge-compensation of the aliovalent solute by lithium vacancies; in the purely vacancy-compensated limit, the vacancy concentration is given by $(n-1)[M^{n+}] = [V_{Li}']$. Thus the three doped samples have the compositions $Li_{0.90}Mg_{0.05}FePO_4$, $Li_{0.80}Zr_{0.05}FePO_4$, and $Li_{0.70}Zr_{0.075}FePO_4$ and vary systematically in the concentration of charge-compensating Li vacancies: 5, 15, and 22.5% in the limit of a complete solid solution, respectively. Note that both the dopant and its charge-compensating Li vacancies represent permanent defect concentrations in the crystal − these lithium vacancies cannot be removed even when the material is completely discharged, without violating charge neutrality in the compound. Upon charging, additional lithium vacancies are produced on top of this background population of point defects.

Evidence for this defect model (along with other possible charge compensation schemes) was presented in detail in ref 9. In the case of Mg doping in particular, a distinction is noted between cation ratios that simply allow for isovalent substitution of Mg^{2+} for Fe^{2+}, and those that produce lithium vacancies for charge compensation of divalent cations on the M1 site. A composition $Li_{1-2x}Mg_xFePO_4$, in which Mg^{2+} is an aliovalent solute since either it or Fe^{2+} is forced to substitute for Li^+ on the M1 site, is not the same as a composition $LiFe_{1-x}Mg_xPO_4$, in which Mg^{2+} is an isovalent substitution for Fe^{2+}. Both of these compositions were made and characterized in our recent study,[9] and their lattice parameters shown in Figure 1 of ref 9 distinguish these two solid solutions from one another. X-ray diffraction of the composition $Li_{0.90}Mg_{0.05}FePO_4$ showed no detectable impurity phases.

For the Zr added samples, the predominant phase is the olivine, although vague "shoulders" around the peak at 30° 2θ do not allow us to rule out the presence of trace $Fe_2P_2O_7$.[9] The olivine lattice expands nearly linearly upon doping with up to 12% Zr for the present doping mechanism whereby Zr occupies the M1 site and is charge-compensated by Li deficiency. Refinements of diffraction data (X-ray and neutron) to determine site occupancies confirmed this mechanism in a sample of overall composition $Li_{0.80}Zr_{0.05}FePO_4$, and showed that 86% of the total added Zr was in solid solution. With increasing Zr content, a NASICON phase does become detectable and grows in amount. The peak positions for this NASICON phase shift slightly to lower angles with increasing overall Zr doping level, suggesting an evolution in composition from $Li_2FeZr(PO_4)_3$ toward the pure Zr NASICON $LiZr_2(PO_4)_3$. However, it is emphasized that the appearance of a secondary phase in a multicomponent system, such as this Li−Zr−Fe−P−O system, does not mean that the solubility limit of the olivine has been exceeded, as is explained in detail in ref 9.

Each of the powder samples was fabricated into electrodes having an active material loading of ~3 mg/cm^2 using a formulation consisting of 79 wt % positive active material, 10 wt %

(13) Kang, B.; Ceder, G. *Nature*. **2009**, *458*, 190.
(14) Chung, S. Y.; Bloking, J. T.; Chiang, Y. M. *Nat. Mater*. **2002**, *1*, 123.

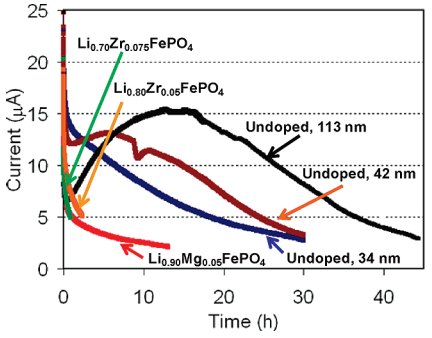

Figure 1. Current vs time for six samples compared in this study, each measured at a constant potential corresponding to the open-circuit voltage at 50% state of charge. Measurements are taken upon a 10 mV step up in voltage from the previous PITT voltage, during the first charge cycle of each sample. A wide range of behavior from rapid purely diffusional response to slow nucleation and growth is observed.

conductive carbon black (Super P, MMM Carbon, Brussels, Belgium), and 11 wt % binder (Kynar 2801). The electrodes were tested in lithium half-cells of Swagelok type, using Arbin or Maccor or Bio-Logic instrumentation. Tests were also performed using electrode formulations having much higher conductive carbon content (65%) to ensure that electrode formulation is not affecting the PITT tests. Those results are not shown here but are indistinguishable from those presented herein. In the PITT measurements, a "staircase" voltage profile was used in which the cell voltage was raised in 5 mV increments, and the current vs time, $I(t)$, was measured at constant potential at 0.05−0.2 s intervals depending on the rate of current decay in the particular sample. Each individual titration was terminated when the absolute current reached a $C/100$ or $C/200$ rate. Galvanostatic discharge capacities were measured by charging the half-cells at a $C/2$ rate to 3.8 V and holding at constant voltage until the current decayed to $C/25$, followed by galvanostatic discharge at the desired rate (up to a $50C$ rate) to a lower cutoff voltage of 2.0 V.

Results and Discussion

To illustrate the wide range of kinetic responses seen among this group of materials, we compare in Figure 1 the current vs time response, $I(t)$, measured for each of the six samples at the potential where the largest increment in capacity is observed. If a lithium miscibility gap is present, the capacity at this potential includes that obtained by the first-order phase transition. From the current relaxation time scales and the form of the curves, it is clear that the rate-limiting steps differ qualitatively and quantitatively between samples. The fastest current relaxation occurs for the three doped samples. As we will show, lithium transport is mostly diffusion-limited for these materials. Among the undoped samples, as the particle size increases, the relaxation curve increasingly takes on the characteristics of a nucleation and growth limited transformation, with a local maximum occurring in $I(t)$ that does not appear in a single-phase diffusion model. This is indicative of a nucleation and growth limited transformation, and is similar to behavior previously seen in $Li_xMn_2O_4$.[15] Comparison of the $I(t)$ response for the three undoped samples shows that reduction of particle size increases the rate of this response as well. A methodology for the quantitative separation of $I(t)$ into diffusive and nondiffusive contributions is presented later.

In Figures 2 and 3, the PITT voltage steps and corresponding current relaxation curves are shown for each of the samples. The voltage curves appear smooth at the scale of Figures 2 and 3 but are composed of 5 mV voltage steps. Likewise, individual current curves, $I(t)$, can be resolved only when the absolute rate is slow, but are composed of a high density of individual measurements. Differences in behavior between samples are easily recognized from the $I(t)$ patterns. We emphasize two main points in these data. First, the current relaxation behavior has markedly different behavior and characteristic times in the single phase region versus the two-phase (voltage plateau) region. For example, the undoped samples in Figure 2 A, B, D, and E show, at low SOC, diffusion-limited relaxation corresponding to the existence of a solid solution field, then a transition to a phase-transition-limited process on the constant-voltage two-phase plateau at intermediate SOC. At high SOC, there is a transition to diffusion-limited behavior again. This behavior is consistent with the existence of a miscibility gap bounded at low and high Li concentration by solid solution fields, and as we have previously shown,[4] PITT can be used to establish the boundaries of the miscibility gap. The absolute rate of current relaxation differs significantly between the solid solution and two-phase regimes. With decreasing particle size, the width of the "two-phase plateau" decreases, and thus the transitions to the slower two-phase kinetics also depend on the particle-size influence on Li miscibility gap. In contrast to this behavior, the two Zr-doped samples in Figure 3B, C, E, and F show, upon charge, diffusion-like current relaxation profiles, indicating predominantly solid solution behavior. The voltage curves for these samples also show a continuous variation of voltage with SOC indicative of a single-phase solid solution. The undoped, 34 nm particle size sample (Figure 2C, F), and the Mg-doped sample (Figure 3A, D) show intermediate behavior.

Another kinetic feature can be observed in Figures 2 and 3: the current flow patterns upon charge and discharge are not necessarily symmetric. Comparing the charge and discharge curves in Figure 2, the phase transformation rate upon discharge appears to be considerably faster than that upon charge. Figures 2A and 2D illustrate this feature most clearly; the time constant for current relaxation on the two-phase plateau is more than twice as long as it is during discharge. This behavior may be related to differences in geometrical or morphological configuration of phases during charge and discharge causing differences in the strain energy that must be overcome for phase propagation. When the response is primarily diffusion-limited, as for the samples in Figure 3,

(15) Levi, M. D.; Gamolsky, K.; Aurbach, D.; Heider, U.; Oesten, R. *J. Electrochem. Soc.* **2000**, *147*, 25.

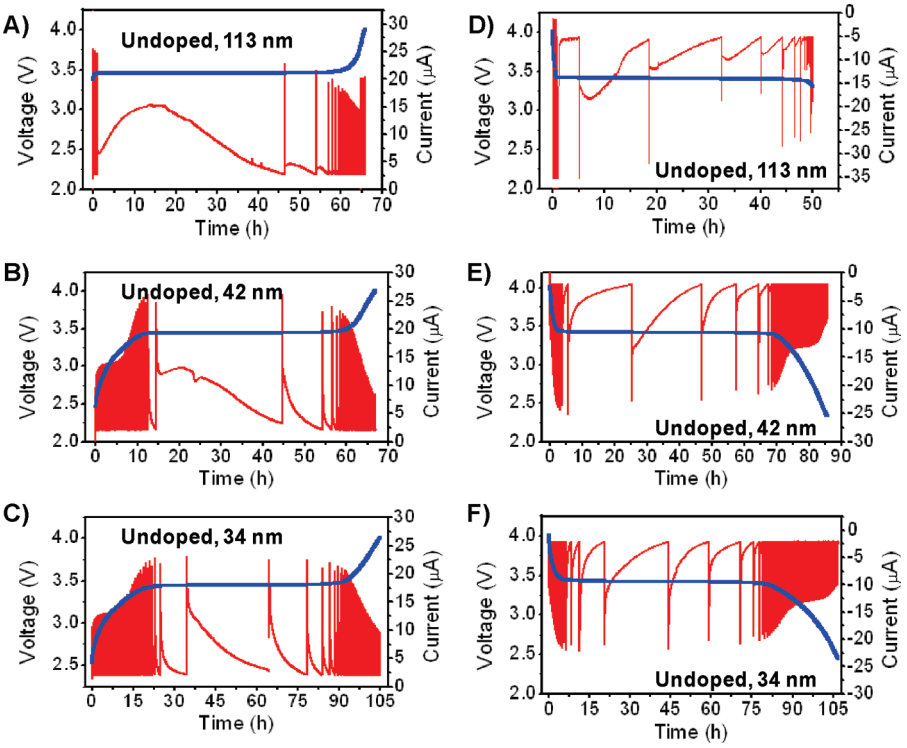

Figure 2. PITT measurements upon (A−C) charge and (D−F) discharge for undoped $Li_{1-x}FePO_4$ of varying average particle size from 113 to 34 nm. Here and in Figure 3, the voltage curves (blue) are composed of 5 mV constant-voltage steps, on each of which the current (red) is measured at 0.05−0.2 s intervals until it decays to a value corresponding to a $C/100$ to $C/200$ rate. Note that with decreasing particle size, the width of the "two-phase plateau" on which the kinetics are phase transformation limited decreases, indicating a shrinking Li miscibility gap.

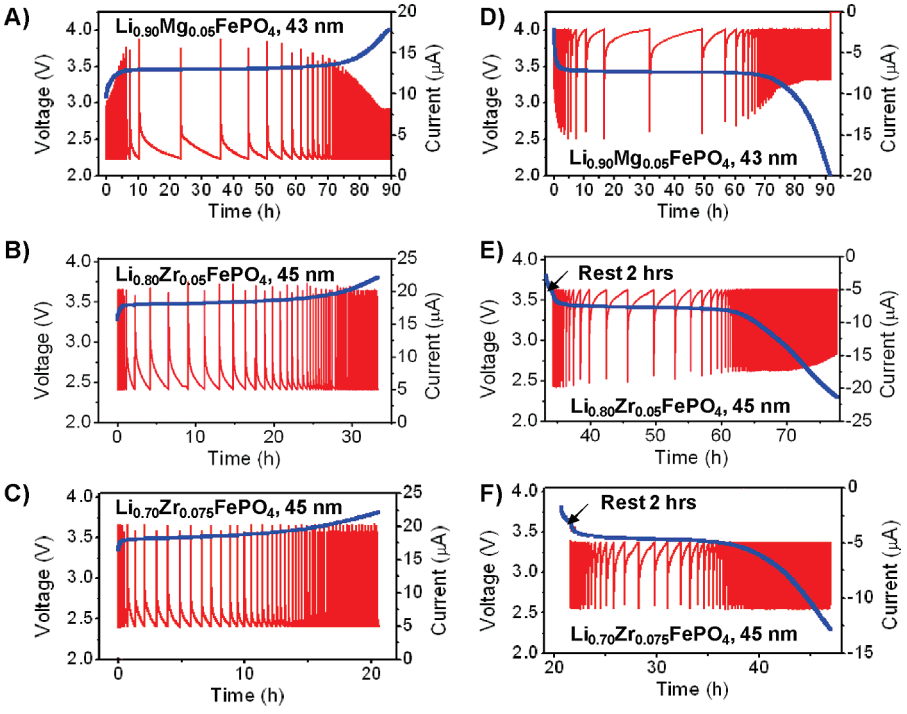

Figure 3. PITT measurements upon charge (A−C) and discharge (D−F) for three aliovalent-doped compositions of nearly identical particle size (43−45 nm). The doping scheme produces systematically increasing concentrations of charge-compensating Li vacancies of 5, 15, and 22.5% respectively. Compared to an undoped sample of identical particle size, Figure 2B and 2E, each of the doped samples shows more rapid kinetics of diffusion-dominated character. As the total defect concentration (dopant + charge compensating vacancies) increases, the miscibility gap disappears and complete solid-solution behavior is observed. Note that the absolute capacities decrease with increasing Li site doping, however, which is attributed to blocking of the one-dimensional Li diffusion channels in the olivine structure.

the current relaxation curves do tend to be more symmetric between charge and discharge.

We note that the asymmetry between charge and discharge kinetics that we see here is opposite to that

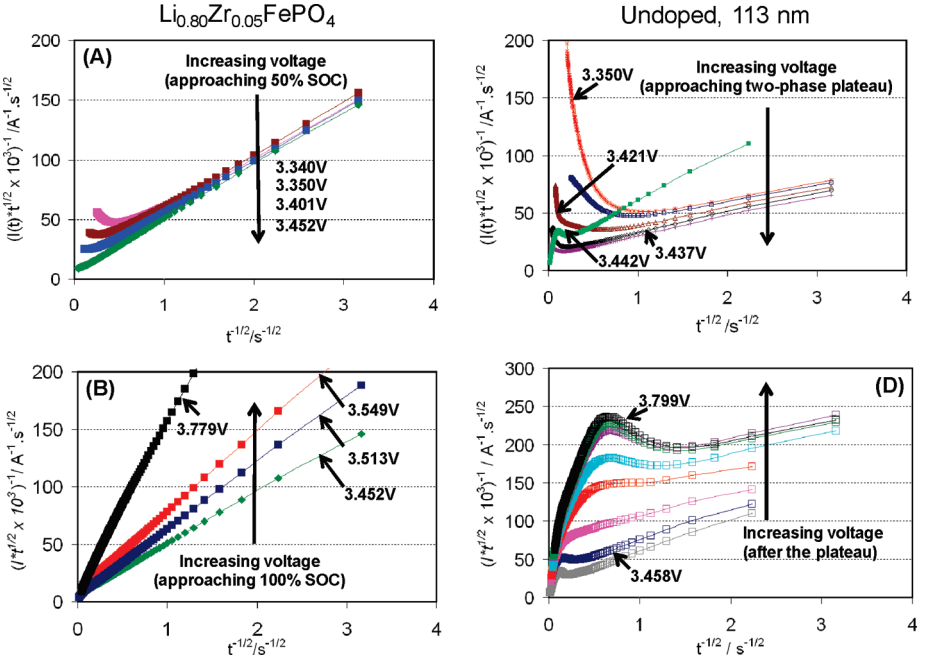

Figure 4. Analysis of potentiostatic responses, here illustrated for two samples during their first charge cycle. Where a diffusion-limited response is present, the short-time current vs time, $I(t)$, can be fit to a two-term model[17,18] from which the lithium chemical diffusion coefficient, D, and a kinetic parameter, Λ, are obtained. (A, B) For the $Li_{0.80}Zr_{0.05}FePO_4$ composition, the good linear fit at all potentials both below and above the 3.452 V potential corresponding to 50% SOC indicates a predominantly diffusion limited response across the entire state-of-charge range. This sample exhibits a nearly complete lithium solid solution. (C, D) Undoped sample of 113 nm particle size, for which nucleation and growth dominate the kinetics on the two-phase voltage plateau. Nonetheless, there is a short-time diffusive response at all potentials from which a value of D can be obtained. The actual capacity obtained from this diffusive response may be exceedingly small, as discussed in the text.

observed by Srinivasan and Newman.[16] At a constant current density, they observed higher utilization upon charge than upon discharge, and attributed the differences to a core−shell configuration in which slower Li diffusion through the lithiated shell during discharge results in the lower utilization. The reason for the different behavior from our samples is not clear. We have previously noted[6] that elastic strain energy minimization in a two-phase particle does not favor the core−shell configuration. Nonetheless, actual behavior may depend on particle size; the particle size of their materials was not given so we cannot make a direct comparison with any of the present samples.

For the six samples, we obtained a total of more than 2500 $I(t)$ curves, each of which was then analyzed to obtain the results presented in this paper. In cases where the transport is diffusion-limited, Vorotyntsev et al.,[17] Levi et al.,[18] and Montella[19] have provided clear expositions on how such data may be analyzed to obtain transport coefficients within certain simplifying assumptions. One widely used method extracts a diffusion coefficient using Cottrell's diffusion-only model applied to PITT data. This graphical method[17,18] utilizes a transformation that produces a straight line at early times; assuming that at early times that diffusion dominates the kinetics, the regression of the straight line produces estimates for a characteristic diffusion time $\tau_D = L^2/D$, and the ratio, $\Lambda = R_D/R_{ext}$, of the diffusion resistance to the external resistance. The diffusion coefficient is D and L is a characteristic particle size. This graphical method utilizes the data from the current-decay, $I(t)$, and the total amount of charge transferred, ΔQ^{total}, after a single PITT increment. The diffusion-only model for the current is

$$I(t) = \frac{Q^{total}}{\tau_D/\Lambda + \sqrt{\pi \tau_D t}} \quad (1)$$

A linear regression on a plot of $1/(I(t)\sqrt{t})$ versus $1/\sqrt{t}$ produces a slope and intercept, m and b, from which τ_D and Λ are determined by

$$m = \frac{\tau_D}{\Lambda Q^{total}} \text{ and } b = \frac{\sqrt{\pi \tau_D}}{Q^{total}} \quad (2)$$

Figure 4A and B shows PITT data obtained on charging for the $Li_{0.80}Zr_{0.05}FePO_4$ composition (Figure 3B), plotted in this form. The regression indeed shows a linear relationship, with deviation seen only at long times (close to the origin), where effects of finite-space (non-Cottrellian) diffusion appear. The good fit to linearity, with $R^2 > 0.98$ at all potentials both below and above the 3.452 V potential corresponding to 50% SOC in this sample, indicates a predominantly diffusion limited response across the entire Li concentration range. Thus this sample exhibits behavior characteristic of a nearly complete lithium solid solution.

(16) Srinivasan, V.; Newman, J. *Electrochem. Solid-State Lett.* **2006**, *9*, A110.
(17) Vorotyntsev, M. A.; Levi, M. D.; Aurbach, D. *J. Electroanal. Chem.* **2004**, *572*, 299.
(18) Levi, M. D.; Demadrille, R.; Pron, A.; Vorotyntsev, M. A.; Gofer, Y.; Aurbach, D. *J. Electrochem. Soc.* **2005**, *153*, E61.
(19) Montella, C. *J. Electroanal. Chem.* **2002**, *518*, 61.

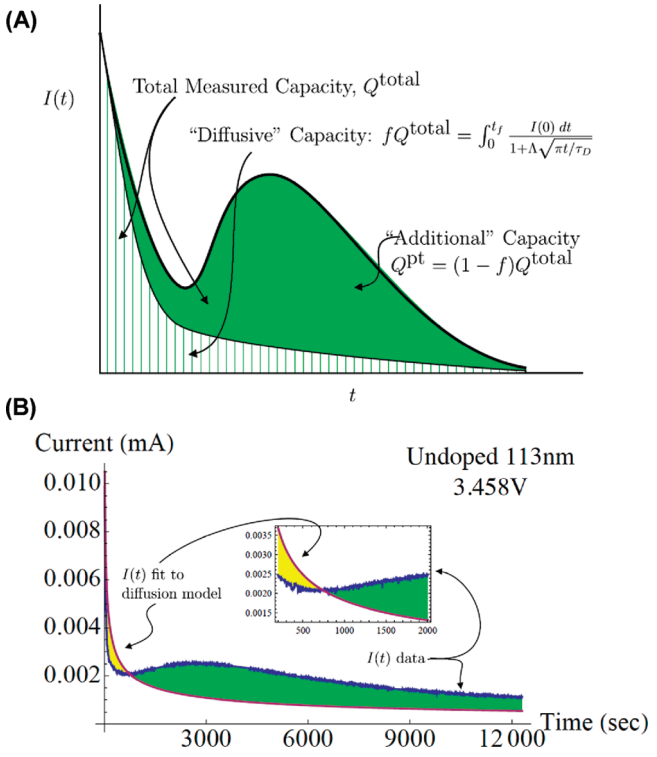

Figure 5. (A) Schematic showing methodology for separating contributions to the total capacity measured at a constant potential by PITT. From the current vs time response, $I(t)$, the "diffusive" capacity is obtained using the analysis of Aurbach and co-workers,[17,18] whereas the additional capacity, which we attribute to the first-order phase transformation, can be obtained by difference. (B) Example for the undoped sample of 113 nm average particle size, measured at the potential yielding the largest capacity in this sample (during the first charge cycle). The yellow region is the difference between the Aurbach fit and the experimental data; it is an indication of how much the semi-infinite Cottrelian model overestimates the observed diffusion.

When the phase transition plays a prominent role, more complex behavior results, as illustrated in Figure 4C and D for the undoped, 113 nm particle size sample. Here there are substantial deviations from the simple diffusion-limited process. It is still possible to obtain a linear regression fit to the short-time response for each of the PITT relaxation curves using the transformation introduced by Montella[19] and used by Vorotyntsev et al.,[17] (i.e., $R^2 > 0.98$). The diffusivity D can be estimated from this regression. However, the actual capacity obtained from this diffusive response may be exceedingly small, in many cases equivalent to less than a monolayer of Li per particle. Therefore, the existence of a diffusive component, which in each of the cases is a faster Li storage/release response than the phase transformation, may be irrelevant compared to stored capacity.

Separating Diffusive Capacity and Phase Transformation Capacity. Separating the short-time diffusive capacity from the long-time, phase-transition capacity is therefore useful for understanding differences in behavior among the respective materials. Our procedure for doing so is illustrated graphically in Figure 5A, with a fit to the data for the undoped, 113 nm particle size sample shown in Figure 5B as an example. When there are other contributions to the capacity, Q^{total}, such as a phase transformation, the diffusion-only model will not suffice. Nevertheless, because short time kinetics are likely to be dominated by diffusion, the Aurbach graphical method might be expected to give a reasonable approximation to τ_D and thus to D. However, only a fraction, f, of the total measured Q^{total} is associated with diffusion: $Q^{\text{diff}} = f\,Q^{\text{total}}$. The remaining transferred charge is denoted $Q^{\text{pt}} = (1 - f)Q^{\text{total}}$. In this case, the Aurbach method should be modified to account for only the diffusive portion of capacity

$$m = \frac{\tau_D}{\Lambda Q^{\text{diff}}} = \frac{\tau_{\text{D}}}{f\Lambda Q^{\text{total}}} \text{ and } b = \frac{\sqrt{\pi\tau_{\text{D}}}}{Q^{\text{diff}}}$$

$$= \frac{\sqrt{\pi\tau_{\text{D}}}}{fQ^{\text{total}}} \text{ or } \tau_{\text{D}} = \frac{b^2 f^2 Q^{\text{total}^2}}{\pi} \text{ and } \Lambda = \frac{b^2 f Q^{\text{total}}}{m\pi} \quad (3)$$

Only two of the three model parameters (f, τ_{D}, and Λ) are determined by the data and graphical method. Another equation may be found by computing the relative contribution of the diffusive capacity to the total accumulated charge. Rewriting the expression for the current for the diffusive capacity and using eq 3

$$I^{\text{diff}}(t) = \frac{fQ^{\text{total}}}{\tau_{\text{D}}/\Lambda + \sqrt{\pi\tau_D}t^{\text{D}D}} = \frac{1}{m + b\sqrt{t}} \quad (4)$$

This contributes fQ^{total} to the total charge.

$$fQ^{\text{total}} = \int_{t=0}^{t_{\text{fin}}} I^{\text{diff}}(t)dt = \int_{t=0}^{t_{\text{fin}}} \frac{1}{m + b\sqrt{t}}$$

$$= \frac{2}{b^2}\left[b\sqrt{t_{\text{fin}}} - m\log\left(1 + \frac{b\sqrt{t_{\text{fin}}}}{m}\right)\right] \quad (5)$$

where t_{fin} is the time at the end of the experiment and at which Q^{total} is measured. The right-hand-side diverges as $t_{\text{fin}} \rightarrow \infty$, but so does $Q^{\text{total}}(t_{\text{fin}})$ diverge as $\sqrt{t_{\text{fin}}}$ in the Cottrell model.Therefore

$$f = \frac{2}{Q^{\text{total}}b^2}\left[b\sqrt{t_{\text{fin}}} - m\log\left(1 + \frac{b\sqrt{t_{\text{fin}}}}{m}\right)\right] \quad (6)$$

Thus, all three model parameters f, τ_{D}, and Λ are determined by eqs 3 and 6.

The parameter f separates Q^{total} measured at each potential step into diffusive and nondiffusive components. The slope and intercept parameters, m and b, in eq 6 were determined with the short-time fit as determined by the Aurbach graphical method. The total charge was determined by integrating the current up to the end-of-titration time, t_{fin}, to find the accumulated charge Q^{total}. From these experimental parameters, the fraction f is determined from eq 6. Results are plotted in Figures 6 and 7 for the samples studied. Figure 6 shows the total capacity, Q^{total} and the diffusive capacity Q^{diff} for undoped samples having average particle sizes of 113 nm, 42 nm, and 34 nm, plotted for both charge and discharge. Results are shown against half-cell voltages, i.e., the potential

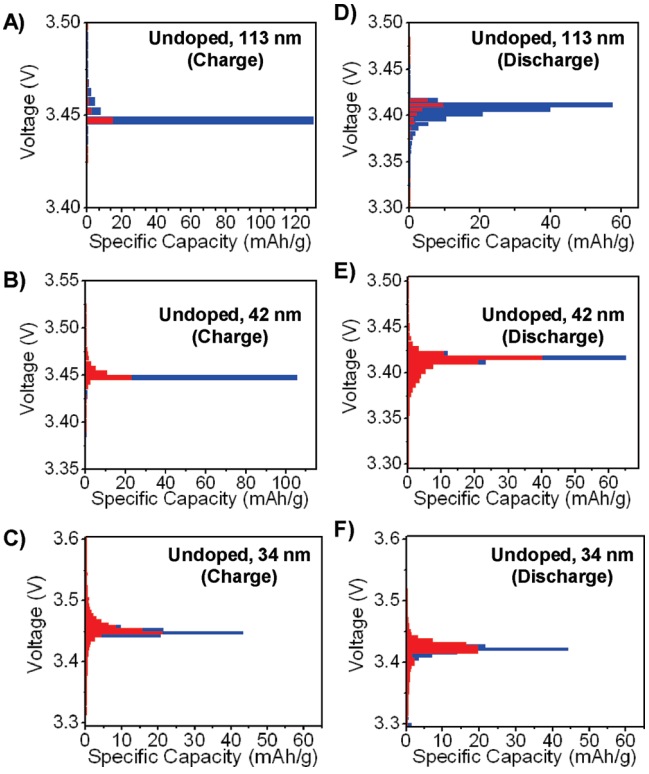

Figure 6. Total capacity, Q^{total} (in blue), and "diffusive" capacity, fQ^{total} (in red), for undoped samples having average particle sizes of 113, 42, and 34 nm, measured upon charge and discharge. Results are plotted against half-cell voltage, i.e., the potential with respect to Li/Li$^+$. The diffusive capacity is in each case accumulated at short times (see Figure 5). The difference between the total and diffusive capacity at each potential, $(1-f)Q^{\text{total}}$, is the capacity accrued as a result of the slower, first-order phase transition. With decreasing particle size in the sequence A−B−C and D−E−F, a larger fraction of the total capacity is diffusive, and the potential range over which significant capacity is obtained is broadened, consistent with a shrinking Li miscibility gap (larger solid-solution field for both the lithiated triphylite and delithiated heterosite endmember phases).

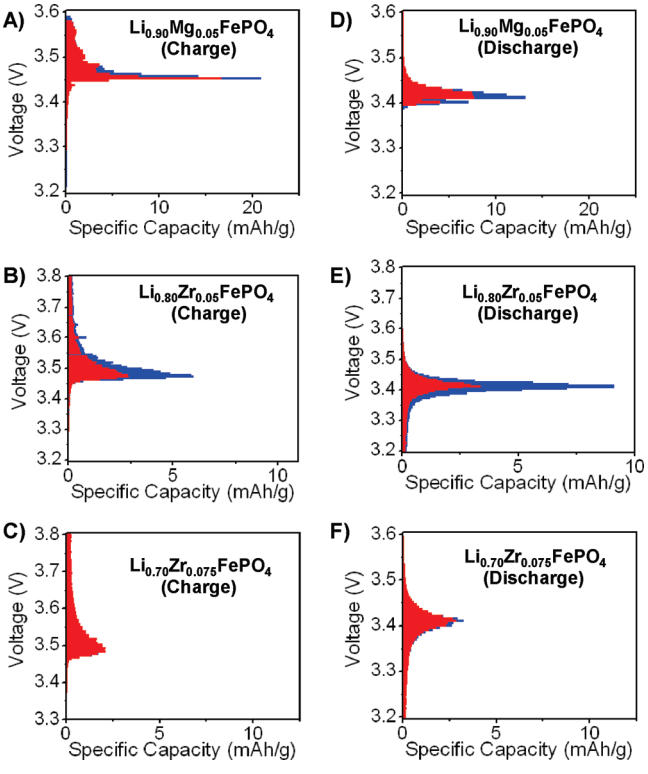

Figure 7. Total capacity, Q^{total} (in blue), and "diffusive" capacity, fQ^{total} (in red), for three aliovalent-doped samples having nearly identical particle size (43−45 nm), measured upon charge and discharge. Results are plotted against half-cell voltage, i.e., the potential with respect to Li/Li$^+$. Note that the relative contribution of the diffusive capacity is in general greater than for the undoped samples in Figure 6, and that significant capacity is accrued over a wider voltage range, consistent with a narrower Li miscibility gap. In the 7.5% Zr-doped sample in particular (C, F), the near-absence of phase transformation capacity is consistent with a complete solid solution at room temperature.

with respect to Li/Li$^+$. The difference between the total and diffusive capacity at each potential may be assigned to capacity accrued as a result of the slower, first-order phase transition, Q^{pt}. With decreasing particle size in the sequence A−B−C and D−E−F, it is clear that a larger fraction of the total capacity is diffusive, and also the potential range over which significant capacity is obtained is broadened. This is consistent with a shrinking Li miscibility gap (larger solid solution field for both the lithiated triphylite and delithiated heterosite phases) as the particle size decreases.[4] Notice also that for the coarsest material (113 nm), which previous work has shown to have nearly complete Li immiscibility, nearly all of the capacity obtained during charge (Figure 6A) occurs at a single potential corresponding to the two-phase plateau voltage.[6] A small phase transformation capacity is obtained at higher potential steps, suggesting that there are particles in this sample which require a higher overpotential for phase transformation. Interestingly, upon discharge, Figure 6D, the phase transformation capacity of this sample is obtained over a broader range of potentials (~50 mV) than during charge. The 42 nm undoped sample shows qualitatively similar behavior on charge (Figure 6B). However, upon discharge (Figure 6E), it is apparent that the phase transformation capacity is proportionally less and now constitutes a minority of the total capacity. The apparent width of the miscibility gap is also narrower—and the kinetics faster—during discharge than during charge of the same sample. This was also suggested by the $I(t)$ curves for this sample in Figure 2. The asymmetry in behavior may be related to irreversible changes taking place during cycling, such as the creation of defects that lower the nucleation barrier for subsequent phase transformations. The results emphasize the fact that the electrochemical response of fine particle olivines is typically history-dependent. Changes in nucleation and growth kinetics upon repeated cycling, especially for larger particle sizes in which damage accumulation is likely more severe, are interesting and deserve further study.

In the undoped samples, Figure 6, even at the smallest particle size (34 nm) there remains a substantial phase transformation capacity occurring near a single potential corresponding to the first order phase transition. This is consistent with there being Li immiscibility even at the smallest size scale represented here. The aliovalent doped samples, Figure 7, show further evolution toward complete solid solution behavior. Here the total capacity, Q^{total} (in blue) and the diffusive capacity Q^{diff} (in red), are

plotted for the three aliovalent-doped samples of nearly identical particle size (43−45 nm), measured upon charge and discharge. Note that the relative contribution of the diffusive capacity is in general greater than for the undoped samples in Figure 6, and that significant capacity is accrued over a still wider voltage range, consistent with a further reduced Li miscibility gap, especially when compared to the undoped sample of nearly identical particle size, 42 nm, in Figure 6B and E. In the 7.5% Zr-doped sample in particular (Figure 7C, F), the near-absence of phase transformation capacity is consistent with a complete lithium solid solution existing at room temperature. The difference in behavior between the 5% and 7.5% Zr-doped samples is furthermore consistent with differing amounts of dopant in solid solution. This supports the results of Meethong et al.[9] where, on the basis of structural analyses, it was concluded that the Zr solid solubility in the olivine phase continues to increase well beyond a few percent when the composition is formulated to accommodate charge-compensating vacancies.

Chemical Diffusion Coefficients. The lithium chemical diffusion coefficients obtained from the PITT data using the linear regression method are shown in Figure 8 for each of the six samples. The results are plotted against the voltage at which the $I(t)$ response was measured. Each plot includes results obtained upon charge as well as discharge. Furthermore, we have superimposed against the diffusion coefficient values the capacities, Q^{total}, measured at each potential upon charge and discharge. The trends exhibited by these results raise several interesting questions, and illustrate inherent limitations in the application of diffusion models to materials that primarily store charge via phase transformations. It is to be emphasized that the D values plotted here are obtained from $I(t)$ data that satisfy previously established criteria for the kinetic analysis; diffusion coefficients are not being obtained from regimes of behavior that are obviously nucleation and growth limited. Furthermore, for self-consistency the capacity used to obtain D is the diffusional capacity Q^{diff} and not the total charge capacity at the measurement potential.

One clear trend exhibited by the data is an apparent minimum in D occurring at potentials where the capacity obtained per increment of voltage in the PITT measurements is the largest. The minimum value of D ranges from 1×10^{-14} cm^2/s to 1×10^{-17} cm^2/s depending on the sample in question, and the state of charge of the material is typically about 50% SOC at this potential. The appearance of a minimum in D where incipient or actual first order transitions occur has been previously observed in several materials,[20,21] including $LiFePO_4$.[22] This effect may be understood from the point of view that a system

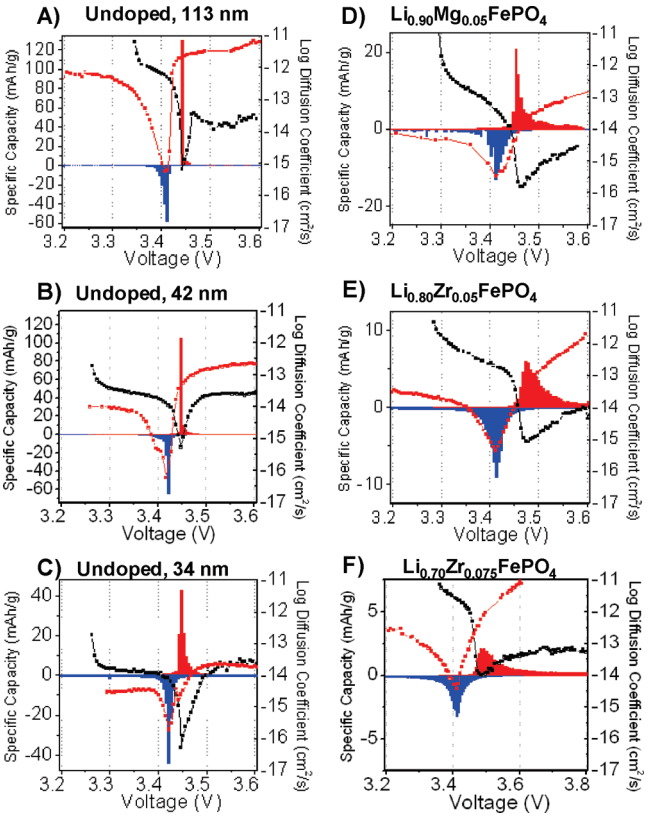

Figure 8. Chemical diffusion coefficients obtained from PITT data using the analysis illustrated in Figure 4, plotted against the voltage at which the $I(t)$ response was measured, for each of the six samples in this study. Results obtained upon charge (black curves) and discharge (red curves) are shown. Superimposed against the diffusion coefficients are the charge capacities, Q^{total}, measured at the same potential upon charge (red histograms) and discharge (blue histograms), respectively. See text for detailed discussion.

which is about to phase separate into Li-rich and Li-poor regions will exhibit local aggregation of Li ions and Li vacancies, thereby reducing the lithium diffusion coefficient compared to the instance of randomly distributed vacancies. Away from the minima, the D's are higher by several orders of magnitude, reaching values as high as 1×10^{-11} cm^2/s in the present materials. However, examination of the capacity available at these potentials shows that, despite there being adequate current flow for the diffusion kinetics to be modeled, there is in reality very little capacity available. Although not resolvable in Figures 6 and 7, these capacities are generally equivalent to less than a monolayer of Li per particle, at the particle sizes used in these experiments. Clearly, a high value of D is only meaningful if significant capacity can be accumulated by the diffusive process in question; there is no practical value to high diffusivities that accrue negligible capacity. Furthermore, one cannot be certain that these values of D represent lattice diffusion in the olivine structure as opposed to, for example, accumulation in a surface layer.

In addition, when diffusion coefficient values are obtained in regimes where the phase transformation is active, as is clearly the case for the undoped samples (Figure 8A−C), one should question the assumption that diffusion occurs across the entire particle dimension L.

(20) Levi, M. D.; Gamolsky, K.; Aurbach, D.; Heider, U.; Oesten, R. *J. Electroanal. Chem.* **1999**, *477*, 32.
(21) Levi, M. D.; Aurbach, D. *J. Solid-State Electrochem.* **2007**, *11*, 1031.
(22) Prosini, P. P.; Lisi, M.; Zane, D.; Pasquali, M. *Solid State Ionics* **2002**, *148*, 45.

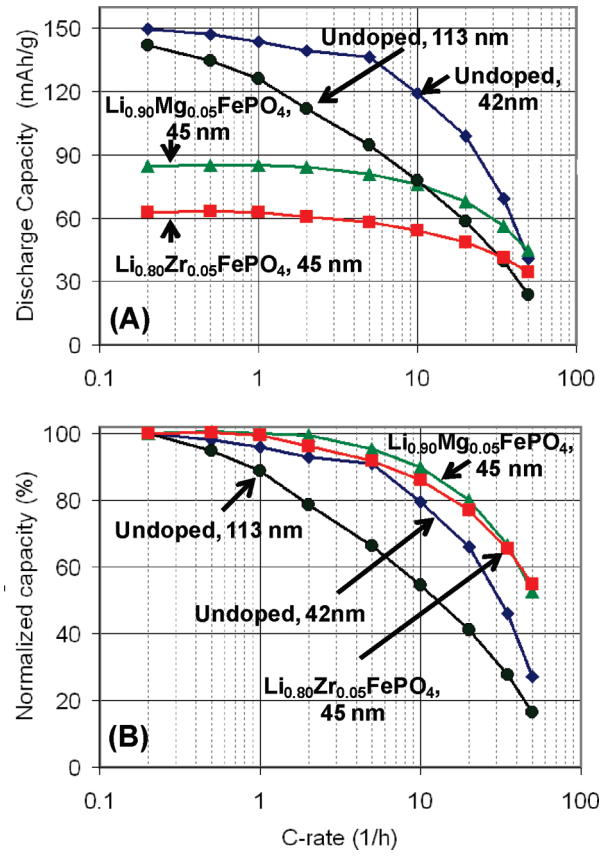

Figure 9. Comparison of specific discharge capacity (mA h/g) vs *C*-rate for samples of 42−45 nm average particle size and various compositions. Compared to the undoped sample, 5% Mg- and 5% Zr-doped samples exhibit decreased capacity at low rates (A), but retain a greater fraction of the low-rate capacity at high rates up to 50*C*. An undoped 113 nm particle size sample is shown for comparison. All samples are prepared as electrodes with 79% active material, 10% conductive carbon black, and 11% binder.

Given that the phase transformation has not yet propagated during the short time regime from which the diffusion coefficients are obtained, it is possible, even likely, that diffusion is occurring over a length scale much smaller than the particle size. We do not know these dimensions−but must regard the diffusion coefficients obtained under such conditions with suspicion given that the value obtained is proportional to the assumed value of L^2; if the effective size of the diffusion region is 1/10th the particle size, the apparent diffusion coefficient will be 1×10^2 lower. Nevertheless, the data presented in this paper are indicative of the relevant time scales and provide a benchmark against which any microstructural model should be evaluated. We note that the minima in *D* are particularly sharp for those samples in which the phase transformation is rate-limiting. Thus it is possible that incorrect assumptions regarding the diffusion length scale are also contributing to the minimum in *D*.

Under those conditions where the analysis shows that the stored capacity at a particular potential is both significant and occurs primarily through a diffusion-limited process, comparisons of *D* seem warranted. This is the case in the doped samples (Figure 7). (Although the possibility of a phase-transformation process that coincidentally exhibits Cotrellian kinetics cannot be completely ruled out.) Comparing panels D−E in Figure 8, there is measurable stored capacity over a wide range of potentials. Even neglecting the minimum values of *D* obtained at the potential corresponding to the peak capacity (where although not resolved, some phase transformation limited capacity may interfere), there are systematic variations among the doped samples. Taking the results upon discharge (red curves) in Figure 8, the range of *D* where the majority of the capacity is recorded (blue histogram) in Figures 8D and 8E is 1×10^{-14} to 1×10^{-15} cm^2/s, but in Figure 8F the value of *D* over the same potential range is more than 10 times higher at 1×10^{-12} to 1×10^{-14} cm^2/s. We note that at the states of charge for which these values of *D* are obtained, the absolute Li vacancy concentrations differ between samples by less than a factor of 2. The much larger difference in Cottrellian *D* suggests that the Li migration activation energy itself has decreased. Such an effect was suggested for materials doped by the present defect mechanism, based on changes in bond lengths compared to undoped materials.[9]

Figure 9 compares the galvanostatic discharge capacities, and the relative capacity retention, vs *C*-rate for samples of 42−45 nm average particle size and various compositions. Compared to the undoped sample, the 5% Mg- and 5% Zr-doped samples exhibit decreased capacity at low rates (Figure 9A), but retain a greater fraction of the low-rate capacity at high rates up to 50*C*. Results for an undoped 113 nm particle size sample are shown for comparison; it loses capacity much more rapidly with increasing rate. Consistent with previous results,[6,9] we see that aliovalent doping improves rate capability through faster kinetics, but at the expense of reduced capacity. It is to be emphasized that we report results on these highly doped compositions not to advocate their practical use but clarify the effects of nanoscaling and doping on the storage mechanisms. The optimal compromise between effects on miscibility gap reduction and capacity reduction due to [010] channel blocking depends on the particle size and the dopant in question; for most applications, it will occur at particle sizes of a few nanometers and doping levels below 5%. Nonetheless, it is possible that powders engineered to maximize the rate of the diffusive response could be used in batteries designed for maximum power at the expense of energy. Although the results presented herein are for electrodes of a relatively standard "high energy" formulation (79% active material, 10% conductive carbon black, and 11% binder), electrodes prepared with much higher conductive carbon content analogous to those recently reported by Kang and Ceder[13] do produce excellent capacity retention at rates as high as 600*C*.

Conclusions

Crystallite size and composition effects on the kinetics of lithium storage in olivines have been studied using potentiostatic intermittent titration tests (PITT) performed

on undoped $Li_{1-x}FePO_4$ of varying particle size, and aliovalent solute doped compositions of varying composition but nearly identical particle size. Using more than 2500 potentiostatic measurements of current relaxation performed on six materials, we show that the kinetics of lithium insertion depend strongly on the instantaneous composition with respect to the lithium miscibility gap. In solid solution fields lying outside of the two-phase voltage plateau, the kinetics are rapid and correlate with a diffusional contribution to the stored Li concentration, or capacity. Within the plateau, the kinetics are much slower and provide evidence of a phase-transformation component to capacity. The graphical method of extracting relative diffusional and external resistance and characteristic time constants can be used when, at early times, the kinetics are dominated by diffusion. In these cases, the contribution of diffusive capacity can be estimated by integrating the Cottrell diffusion model. The difference (between this inferred capacity and the total integrated current $I(t)$ in a single PITT step) can be associated with a remaining capacity which may be assumed to be that of a phase transformation.

Separating the diffusive and phase transformation contributions to stored capacity reveals the impact of particle size and doping. Because the width of the miscibility gap depends on particle size, and on the concentration and type of aliovalent dopant, there is a direct contribution of such equilibrium miscibility gap-reducing effects to faster kinetics. Reducing the width of the miscibility gap by one or both effects, in some cases resulting in a complete lithium solid solution at room temperature, allows the majority of stored capacity to be accomplished using the (faster) diffusive process, while also increasing the rate of phase transformation at lithium concentrations within the miscibility gap. The results also provide evidence for increased diffusion coefficients in aliovalent-doped samples.

Acknowledgment. This work was supported in part by United States Advanced Battery Consortium Project DE-FC26-05NT42403. N.M. acknowledges support by the Khon Kaen University and Thailand Research Fund and Y.H.K. acknowledges support by Taiwan Merit Scholarship TMS-94-2-A-019.